Cubesats for monitoring atmospheric processes (CubeMAP): a constellation mission to study the middle atmosphere

CubeSats for Monitoring Atmospheric Processes (CubeMAP): a constellation mission to study the middle atmosphere

Damien Weidmann*[a], Kelly Antonini[b], Daniel Martinez Pino[b], Bertel K. Brodersen[b], Gayatri Patel[a], Michaela Hegglin[c], Christopher Sioris[d], William Bell[e], Kazuyuki Miyazaki[f], Lars K. Alminde[b], Antonio Gabriele[g], Massimiliano Pastena[h], Alex Hoffmann[h]

[a]Space Science and Technology Department (RAL Space), STFC Rutherford Appleton Laboratory, Harwell Campus, Didcot, Oxfordshire, OX11 0QX, UK; [b]GomSpace, Langagervej 6, 9220 Aalborg Øst, Denmark; [c]University of Reading, Whiteknights, Reading, Berkshire, RG6 6AH, UK; [d]Environment and Climate Change Canada, 4905 Dufferin St, Toronto, Ontario M3H 5T4, Canada; [e]ECMWF, Shinfield Park, Reading, RG2 9AX, UK; [f]Jet Propulsion Laboratory, California Institute of Technology, 4800 Oak Grove Drive, Pasadena, CA 91109, USA; [g]Moltek, Space Business Innovation Centre, Kapteynstraat 1, 2201BB, The Netherlands; [h]ESA, ESTEC, Keplerlaan 1, NL-2200 AG Noordwijk, The Netherlands

ABSTRACT

Some aspects of the CubeMAP mission (also known as ESP-MACCS) are presented: its science objectives, and the key choices made to address these from small satellite platforms. The science case, addressing some key scientific questions related to global change, is elaborated into four questions focused on upper troposphere and stratospheric composition and its change. The sounding choices and the associated observation concept retained is a constellation of miniature limb solar occultation thermal infrared sounders, offering the advantages of limb solar occultation, whilst mitigating the inherent lack of coverage of this geometry. The mission focuses on tropical regions as the gateway to the upper troposphere, and the stratosphere. The miniaturized instrument payloads developed for the mission are briefly presented: the High resolution InfraRed Occultation Spectrometer (HIROS) and the Hyperspectral Solar Disk Imager (HSDI). Lastly, the nanosatellite 12U platform and its subsystem are described completing the overview of the mission space segment.

Keywords: Cubesat constellation, atmospheric remote sensing, high resolution spectrometers, limb sounding. Atmospheric processes.

1. INTRODUCTION

Within the context of the ESA SCOUT program dedicated to developing Earth Observation science mission using small satellite platforms, the CubeMAP mission (also known as ESP-MACCS) has been proposed and retained as one of the four mission candidates to be consolidated.

Earth is changing at an unprecedented pace. Understanding and quantifying the processes driving the change and particularly the role played by the atmosphere is necessary, and the CubeMAP mission has been designed to address this need. The overall mission goal is to study, understand, and quantify processes in the tropical Upper Troposphere and Stratosphere (UTS), study its variability, and contribute to trends analysis in its composition and its effects on climate and vice-versa. The UTS composition plays a significant role in controlling the Earth's climate, with still poorly explored feedbacks within the Earth System. This region of the atmosphere is coupled to the surface and the free troposphere both dynamically and radiatively. Its composition is determined by anthropogenic emissions of greenhouse gases and pollution precursors and is subject to changes via radiative, dynamical, and chemical processes.

*damien.weidmann@stfc.ac.uk

Addressing these demanding science needs has traditionally been the scope of very large scientific missions, using high performance large instruments and buses. The advent of small satellite platforms, which allow for higher agility and cost-effectiveness, offers opportunities to rethink ways valuable science missions can be implemented. CubeMAP contributes to that effort by proposing a mission delivering significant middle atmosphere scientific output using a 12U satellite constellation. The sounding precision and accuracy is ensured by using solar occultation for atmospheric transmittance measurements. The traditional coverage limitation associated to solar occultation is mitigated by the use of constellation flying: three identical spacecrafts are considered. The use of small satellite is enabled by novel payload instruments maintaining an excellent performance vs. size and mass trade-offs.

Section 2 elaborates the specific science objectives of the mission, related to middle atmosphere processes. Section 3 briefly describes the observation concept and the coverage it provides. Section 4 and 5 respectively deals with the instruments part of the science payload and the satellite platform developed for the bus.

2. SCIENCE QUESTIONS CUBEMAP ADRESSES

CubeMAP focuses in the quantitative understanding of processes occurring in the middle atmosphere, defined in this context as composed of the UTS, further split into two regions: the Upper Troposphere/Lower Stratosphere (UTLS) and the stratosphere (S). These regions of the atmosphere, as much as the whole Earth, are subject to change owing to the activities of humankind, changes whose impact requires quantitative understanding. The mission further focuses on the tropical regions as its first component, as Upper Troposphere (UT) to Stratosphere (S) injection is primarily driven by tropical deep convective uplift. They are also the most important source of global biomass burning and mineral dust. The tropics cover half of the globe, with uncertainties in process knowledge being considered to be largest in this region[1].

The UTLS is an exchange and coupling layer between the turbulent free troposphere and the stably stratified stratosphere. Radiative, dynamical, and chemical processes occurring in the UTLS strongly affect the near-term predictability of the climate system. Indeed, surface climate and climate feedbacks are particularly sensitive to the composition and temperature change in this layer[2,3]. Because of the relative minimum temperature in this region, it plays a critical role in controlling the Earth's outgoing long-wave radiation[4]. The UTLS is also hypothesized to play a key role in stratosphere-troposphere coupling, such as during stratospheric sudden warming events that affect surface weather for months after they have occurred[5, 6]. However, the exact mechanism of how the coupling works and how it could be used to enhance predictability of weather is still an open question[7]. Importantly, the tropical UTLS is considered as the gateway into the stratosphere and controls the amount of both long-lived greenhouse gases (H2O, CH4, N2O, and CFCs), medium-lived (CO), and Very Short Lived chemical Species (VSLS) from both human and natural sources passing through the tropopause. In particular, VSLS have been recently pointed out as likely and potential future threats to the stratospheric ozone layer[8]. The Asian monsoon may play an important role in accelerating the transport of such VSLS into the lowermost stratosphere[9]. As such, changes in the UTLS may trigger further changes to stratospheric chemistry and climate.

The stratosphere is less variable than the UTLS. It contains the ozone layer, which shields the Earth from the harmful effects of ultraviolet radiation and affects the Earth's radiation balance. Changes in stratospheric radiatively active species (and in particular ozone, water vapour, and carbon dioxide) affect the temperatures and, through thermal-wind balance, also the winds in the stratosphere. The most prominent example for this mechanism is the Antarctic ozone hole, which has influenced the Southern hemisphere surface climate[10], [11]. Stratospheric water vapour content may be an important driver of decadal surface climate change[12] and is strongly coupled to tropical tropopause temperatures, but also to the amount of methane entering the stratosphere. Stratospheric aerosols are another key driver of the radiative balance of the Earth. The main source of injection comes from tropospheric sulphur species and episodic volcanic eruptions. In addition, stratospheric temperature trends are an important fingerprint of human impact on the climate system, and lack of knowledge of changes in water vapour and ozone in the LS (Lower Stratosphere) lead to significant difficulties in attributing that change[13]. Accurate knowledge of stratospheric climatologies and variability is also pivotal in reaping the benefit of climate and numerical weather prediction models, as well as of nadir sounding observing systems.

The UTS is difficult to access on a global scale by in-situ measurements whereas a space-borne infrastructure is ideal to characterize them. Composition changes in these regions are driven by processes including deep convection and Stratosphere Troposphere Exchange (STE). Effects of deep convection and transport pathways of STE are poorly quantified and are a frontier for understanding the composition of the UTLS and the S. This requires the simultaneous measurements of key molecular species and aerosols with high accuracy, high precision, and high vertical resolution.

These include radiatively active gases (H2O, O3, CO2, CH4, N2O), STE tracers (HCN, CO, HDO), ozone chemistry gases (HCl, ClO and BrO), and aerosols and clouds, as well as their precursors (SO2).

Given the programmatic constraint, CubeMAP will focus on the tropical region, which as the gateway to the stratosphere, critically determines the chemistry of the entire stratosphere. In the tropics, the large-scale patterns of tropical tropospheric convection generate large scale waves which propagate into the stratosphere. These waves influence the Brewer Dobson Circulation (BDC) by affecting transport timescales and pathways, determine the tropical tropopause temperatures, and drive one of the main STE pathways.

More precisely, the quantitative understanding of the processes in the UTS raise the specific questions described in the next subsections. Addressing these questions is the focus of CubeMAP.

2.1 How is water vapour in the UTS responding to climate change, and what is its feedback and impact on climate?

Changes of the distributions of water vapour or thin cirrus clouds in the UTLS strongly impact radiative forcing of the Earth's climate and surface temperatures[3] and also LS temperature trends[12], [14]. UT water vapour changes also play an important (and sometime contentious) role in the strength of the water vapour climate feedback that significantly enhances the sensitivity of climate[2]. Despite its importance, processes controlling interannual variability and trends in UTS water vapour are currently not well characterised. Past trends derived from satellite and in-situ balloon observations in fact seem to show opposite signs[15].

Water vapour in the stratosphere is largely controlled by the seasonal cycle of the minimum temperatures in the tropical tropopause region, which determine the minimum water vapour mixing ratio in the ascending branch of the BDC[16]. Another source of stratospheric water vapour is CH4 oxidation[17].The Asian summer monsoon provides an additional large-scale pathway for water vapour entering the stratosphere during northern summer[18]. The vertical gradient of water vapour at the extratropical tropopause also affects local temperature profiles and thus static stability[19, 20, 21] with potential effects on the propagation of gravity waves at the tropopause and, in turn, stratospheric dynamics.

Besides the large-scale ascent in the tropics, production from methane oxidation, and the monsoon, the contribution of UT convection to stratospheric water vapour is still under debate particularly in the lower stratosphere. In addition, transport and mixing at the subtropical jet affect the lower stratospheric water vapour budget. Both processes have a high temporal and spatial variability and thus introduce large uncertainties to trend estimates. Since the radiative effect of water vapour is directly linked to the vertical gradient, this, in turn, introduces a large uncertainty to forcing estimates.

While stratospheric water vapour is projected by chemistry-climate models (CCMs) to exhibit significant increases by the end of the 21st century, the CCMs show a large spread in projected concentrations, implying large differences in radiative feedback effects in these models[22]. Testing model processes with more precise observations than hitherto available and diagnostics that help identify processes behind the changes (e.g., through the use of isotopologues) is needed to constrain the climate feedbacks via stratospheric water vapour changes[1]. A recent study demonstrated the use of such water vapour isotopologues for detection of dehydration at the tropical tropopause and resulting transport signals within the stratosphere[23].

Atmospheric reanalyses, in providing coherent estimates of the global atmospheric state over multi-decadal timescales, provide another widely used tool for the study of climate variability and change, and for testing CCMs[24]. Estimated trends in lower stratospheric temperatures, a key prediction of climate models, are strongly dependent on the representation of the evolving distribution of stratospheric water vapour[25], [26]. Short term advances in this aspect of reanalyses are dependent on improved initialisation and parametrisation of water vapour and methane in the stratosphere. Longer term improvements are dependent upon: a more complete understanding (and representation) of the complex transport processes in the UTLS; developments in the assimilation of water vapour observations in the stratosphere, and; the development of an observing system for stratospheric water vapour. CubeMAP addresses these challenges.

Vertically highly resolved water vapour measurements from satellites are essential to estimate the effect of convection of the water vapour distribution in the UTLS. In combination with precise temperature measurements, cloud top observations and tropopause measures, this significantly improves the quantification of the different transport pathways into the UTS.

CubeMAP aims to quantify vertically resolved water vapour and methane in the UTS and particularly across the tropopause over a period of at least four years to allow interannual variability to be studied with trend-quality data.

Methane observations will thereby help to constrain the contribution of methane oxidation to stratospheric water vapour. The observation of multiple water vapour isotopologues, on the other hand, will help to quantify the processes that control UTS water vapour and thereby improve our understanding of the hydrological cycle, including knowledge on cloud formation and precipitation processes, but alo water supersaturation in the UT and water vapour entering the stratosphere from the UT in the tropics. High vertical resolution profile information in the UTS will in addition help to constrain and validate water vapour fields (and through its radiative effects also temperatures) in climate and Numerical Weather Prediction (NWP) models.

2.2 How does climate change affect stratospheric O3 and its recovery?

While the Montreal Protocol and its controls on O3 depleting substances has proven to be one of the most effective international agreements to date, addressing a major pressing global environmental issue of the 20th century, the O3 layer is facing new threats from a changing climate. Satellite and ground-based measurements start to indicate a recovery of ozone in the upper stratosphere[27], and in the Southern polar vortex in September[28]. However, ozone increase has not yet been detected at global scale in the LS, where the bulk of ozone resides, 20 years after the peak of Ozone Depleting Substances (ODS) in that region. Recent publications even indicate a decrease in ozone in that region[29], [30].

While the reasons for the recent decline may point towards enhanced chemical depletion, either through very short-lived ozone depleting substances (ODSs) that are not controlled by the Montreal Protocol[8] or due to a renewed increase of previously controlled ODSs[31], [32], were able to show that the observed decreases were mainly driven by stratospheric transport and dynamics. The daunting question here remains whether this dynamical trend will persist into the future. Indeed, climate change is expected to lead to changes in the distribution of stratospheric ozone in several ways.

Current Chemistry Climate Model (CCM) simulations indicate that the future evolution of the ozone layer in the 21st century will be controlled not only by the decline of ODS but also by changes in greenhouse gases (GHGs), mainly CO2, CH4, and N2O. The increase of GHG abundances generally cools the stratosphere, which slows down gas-phase chemical ozone destruction cycles and leads to an ozone increase in the upper stratosphere. Another robust feature of CCM simulations driven by GHG increases is an acceleration of the Brewer-Dobson circulation (BDC) that transports ozone towards higher latitudes[33], [34]. Such an acceleration, whose attribution is still a subject of debate, would induce a decrease of ozone in the tropical lower stratosphere and an increase at higher latitudes.

Hegglin and Shepherd[19] showed that an important effect of these changes in stratospheric ozone will increase the ultraviolet (UV) radiation reaching the Earth's surface in the tropics by 5%, and decrease UV at mid to high latitudes in the Northern Hemisphere by up to 10% year-around. The increases in UV in the tropics is of great concern since UV levels are to begin with higher and more people live in the tropics than at higher latitudes, increasing greatly the risk for skin cancer. The large decrease in UV at Northern mid to high latitudes, on the other hand, may cause severe problems for vitamin-D production and human-health, a topic already now identified as a key issue for people living in Northern countries[35]. The findings are in the meantime confirmed by an evaluation based on a larger suite of chemistry-climate models[36].

In addition, these changes may affect stratospheric ozone fluxes into the troposphere, with increases in the Northern hemisphere by up to 30% over this time period, potentially affecting tropospheric air quality, and also leading to a radiative feedback due to the large radiative impact of ozone changes in the UTLS[19].

The role of ozone changes in the UTS region and its influence on radiative forcing is poorly understood and reproduced in climate models. IPCC AR5[37] identified significant uncertainties in radiative forcing (RF) due to ozone change. The central RF estimate for tropospheric ozone increases between 1765 and 2011 is 0.4 W.m-2 but with a 95% confidence level of 0.2 to 0.6 W.m-2. At its upper limit, tropospheric ozone would be the second most important GHG RF after CO2; similarly, stratospheric ozone changes in recent decades have also contributed to RF[38], [39]. Estimates of ozone RF are heavily reliant on model simulations, but there is a dearth of height-resolved measurements in the UT with which to confidently validate them; ozone RF is particularly sensitive to changes in the UT.

While the mechanisms behind the chemistry-climate model predictions and the extent of these impacts still need to be explored in further detail, observations of the real atmosphere over the next few decades and particularly in the tropics are essential to evaluate and gain confidence in these predictions. CubeMAP will contribute to the monitoring of the global O3 layer with an improved coverage dataset compared to a single solar occultation instrument and help quantify how a changing climate, through changes in stratospheric circulation and changing levels of GHG, may affect its natural

balance. Hence the effects of changing UV levels and its effects on the biosphere would be quantified. In addition, CubeMAP will help to identify the key processes in the UT and S region that lead to the changes**.**

2.3 How can we improve surface emission estimates of GHG and surface ozone through improving UTS representation of GHG and O3?

The effectiveness of future emission controls on concentrations of the major GHG, CO2, methane, and O3, will primarily be monitored by nadir sounders with high horizontal resolution, combined with inverse modelling or data assimilation. UTS distributions of these gases however account for a considerable amount of variability and need to be constrained by observations to allow for a more meaningful and accurate source estimation[40].

Emissions of GHGs, such as methane, were estimated based on inversion approaches, mainly using vertical column satellite products from nadir satellite measurements[41]. Since the relationship between surface emissions and measured atmospheric quantities is assumed to be predicted well by the model in the inversions, it is important to represent the transport/chemical processes and tropospheric vertical profiles in a realistic way when estimating the surface emissions. Assimilating limb profile measurements is expected to improve emission estimates, as these reduce model errors unrelated to surface emissions and modify vertical profiles.

The case of GHGs has been made by Houweling et al.[42], who showed the large diversity in the simulated column-average CH4 (XCH4) among models associated with errors in atmospheric transport models, such as in STE, and the large contribution from the stratosphere to the model differences in XCH4. Compared with CO2, stratospheric variability and transport are relatively important for the column-average mixing ratio of CH4 because of the steeper vertical gradient of methane in the stratosphere. Constraining UTS methane from CubeMAP is expected to improve source–sink inversions when combining with nadir satellite measurements, through greatly reduced errors in model representations of stratospheric vertical profiles or facilitating use of tropospheric column averages derived from nadir and limb.

An equivalent problem concerns tropospheric ozone in the tropical region. Currently available estimates of tropospheric partial column ozone from a suite of satellite nadir sounders show large discrepancies in both interannual variability and trends[43]. However, indirect evidence for tropical tropospheric ozone increases between 1960 and 2010 has been obtained by subtracting stratospheric partial column ozone derived from stratospheric limb sounders from ground-based total column ozone measurements, supported by the successful modelling of the respective changes in the stratosphere [44]. The information from the satellite limb sounders (as would be obtained by CubeMAP measurements) thus also provides an important constraint for the a priori profile used in the retrieval process of the tropospheric ozone measurement, exploiting nadir/limb solar occultation complementarity.

CubeMAP will provide the high accuracy CO2, CH4, and O3 profile observations needed in tandem with assimilated UV/VIS (Visible) – TIR (Thermal InfraRed) and SWIR/TIR nadir sounding data to enable improved global/regional emission estimations of GHG and air quality. This will also improve understanding of the chemistry-climate system both in the troposphere and stratosphere and the chemical lifetime of various gases.

2.4 How does the composition of the tropical UTS and its response to increasing anthropogenic and natural emissions change?

Distributions of trace gases in the tropical tropopause region show large spatial and temporal variability driven by complex dynamical, transport, and chemical processes across a range of scales, which makes the quantification of long-term changes difficult[45]. In addition, emission sources in the tropics are currently undergoing significant changes driven by economic growth, particularly across the Asian region. Thus, there is also a challenge to understanding the drivers of long-term change in the tropical UT and S.

Air in the tropical upper troposphere undergoes (on average) continuous and slow ascent, while circling zonally around the globe, during which it is influenced by deep convective transport of air from different source regions[46], [47]. Over the ocean, air depleted in ozone causes low upper tropospheric ozone values, while over land, convection leads to higher ozone values due to concomitant transport of air pollution gases. In addition, stratosphere-troposphere exchange via deep stratospheric intrusions from the extratropical LS also can impact the tropical UT[1].

Recently, the aerosol budget in the tropical UTS has been shown to be influenced by uplift of non-volcanic aerosols, e.g. smoke aerosols due to pyroconvection[48] and pollution aerosols uplifted by monsoon systems in the Northern Hemisphere. In the last two decades a new aerosol layer coined ATAL (Asian Tropopause Aerosol Layer), has developed near 16 km inside the monsoon anticyclone and is attributed to the increasingly polluted sources at the

ground[49], [26]. Recent studies have pointed out that the upper layer circulation of the Asian monsoon has a remarkable impact on the chemical composition of the northern mid-latitude stratosphere, in particular at the end of the monsoon season[50], [51].

CubeMAP will provide new tropical constraints on tropical UTS tracer distributions that will help quantify the influences of deep convection, stratosphere-troposphere exchange (from the extratropics), pollutant transport from the planetary boundary layer via long-range transport and convection, and in-situ sources of reactive chemical species from lightning and aircraft.

3. OBSERVATION CONCEPT

3.1 Limb solar occultation transmittance measurements

The observation techniques retained for CubeMAP is limb solar occultation (LSO). LSO provides high vertical resolution, high sensitivity owing to the high Signal to Noise Ratio (SNR) from the strong solar background radiation making tenuous species measurable. It also warrants the possibility of isotopologue ratio measurements, requiring few per mil relative difference to be resolved. The SNR remains high even when Doppler-limited spectral resolution is required to fully resolve absorption lines in the stratosphere.

Using LSO, a relative transmission measurement is made, which is self-calibrated and remains so over long period of time. By using an exoatmospheric measurement for each occultation and owing to the stability of the Sun as a background source on short timescales, high accuracy can be obtained with instrumental simplicity. This relaxes requirements on the instrument stability, as stability is only required over a single occultation measurement[52].

LSO has a long heritage from the late 1970's up to now. Instruments carrying out LSO include the Stratospheric Aerosols and Gas Experiment (SAGE I, II, and III), the Halogen Occultation Experiment (HALOE), the Polar Ozone and Aerosol Measurement (POAM II and III), SOFIE (Solar Occultation For Ice Experiment), and the still operational Atmospheric Chemistry Experiment (ACE).

In LSO, time can be converted to tangent altitude and vertical resolution is driven by instantaneous instrument's field of view (FoV) and measurement integration time. The FoV needs to be small enough to cope with the apparent decreasing vertical extent of the sun owing to atmospheric refraction at low tangent heights. Typically, for a lower Earth orbit, an occultation event lasts from ~30 s to ~1 min depending on the angle between the satellite-sun vector and the satellite orbital plane. This angle also controls the apparent ascent/descent rate and in turns affects the vertical resolution. Vertical resolution can be very high (~1 km typically) at the expense of the geographic coverage (typically a ~200 km long line of sight when the occultation is aligned to the orbital plane). The longitude/latitude coverage is dependent on orbit inclination and flight altitude. For CubeMAP, the tropics is the area of focus. Two measurements per orbit can be made, at spacecraft sunset and sunrise, leading to ~30 measurements per day per spacecraft. Cycle of coverage (latitude vs time) can be changed depending of the orbit precession rate compared to the sun, which in turns will affect the latitude coverage. The geometry of LSO measurement is illustrated in Figure 1.

Clearly, the high-sounding SNR, the vertical resolution, and the simplicity comes at the cost of temporal and spatial coverage, and to a lesser extent to measurements at solar zenith angle limited to 90 degrees. How can we address the coverage drawback whilst retaining the advantages? CubeMAP proposes to obviate the coverage limitations by flying a constellation of configurable small satellites, whose individual orbits can be optimised to fulfil the science requirements.

LSO has already been proposed from a nanosatellite type of platform[53], and so has the concept of nanosatellite constellation[54] to probe the middle atmosphere using miniaturized multi-spectral radiometers. CubeMAP follows this trend and adds high-resolution transmittance spectroscopy capabilities. This represents a paradigm shift compared to using single large payloads taking large, complex, high specification instruments. The cost of flying a constellation requires significant reduction in volume and mass. It also provides economy of scale when the platform and payloads are modular enough and nearly identical.

To fulfil CubeMAP requirements, the payloads must be miniaturized whilst retaining the high level of spectrometric performance needed for UTS sounding, which is typically antagonistic. We propose using spectrometers that target highly specific and optimized narrow-spectral windows, in which individual spectral lines are fully resolved even in the stratosphere. By selecting individual molecular transitions, the temperature dependence can be minimized (low ground state energy of the transition) or optimized if a proxy to temperature measurement is needed, and measurement dynamic

range can be optimized. Likewise, isotopologue transitions can be optimally selected. Trade-offs between multiple molecular signature and optimum absorption intensities are to be realised. Lastly, the use of narrow spectral windows favours an enhanced control of the error and bias budget (broadband effects, baseline effects, interferences effects…) and ultimately delivers higher accuracy.

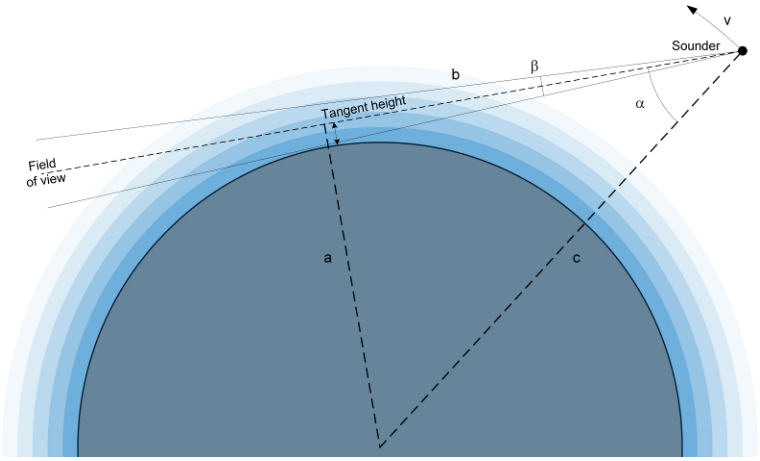

Figure 1. Two dimensional illustration of the LSO geometry where the spacecraft orients itself to catch the atmospheric sunlight transmitted through the atmosphere at sunset and sunrise every orbit. This illustration relates to the particular case where the sun vector is coplanar to the orbit plane.

3.2 Constellation's coverage

The mission science objectives focus on processes in the tropics. Therefore, overall geographical coverage must at the very least span these regions between +/- 25° latitude. This coverage requirement implies low inclination orbit [20-30°] for the satellites. Beyond the latitude extent, the spatial coverage requirements are determined by transport processes on regional to global scales. While convective outflow, biomass burning, and other anthropogenic emissions act more localised, upper tropospheric transport and mixing act to spread the signature of convective transport over vertical and horizontal scales of 1-3 km and 100 s of kilometres, respectively. Resolving processes down to the synoptic scale calls for a spatial resolution in the range of ~500 km. The spatial resolution requirement is therefore set to a 4°x4° latitude longitude grid.

Inherent to the LSO, each tangent point measured to obtained atmospheric profiles will happen at slightly different locations due to the spacecraft motion. This effect is illustrated in Figure 2a, where locations of tangent points from 0 to 100 km are represented within the 4°x4° cell. With this in mind, for the sake of clarity, onwards only the 30 km tangent point will be represented. A one month coverage map for the CubeMAP constellation is represented in Figure 2b, and perhaps more informative, the one month coverage density map is represented in Figure 2c. The coverage density map shows that >90% of the tropics are covered with observations within a month.

If a single 4°x4° cell is considered, an analogue to the revisit time can be derived. This is illustrated in Figure 3 for a cell located on the equator at 90° east. The stick diagram shows the observations occurrence within a year of the mission, the color coding related to the three different spacecraft of the constellation. Revisit time requirement is driven by the UTS variability, which is pronounced both longitudinally and temporally. The longitudinal variations are driven mainly by differences in convective activity over different regions, while temporal variations range from daily, over seasonally, to interannually. To resolve processes at timescales shorter than the seasonal variability a requirement for a full coverage on a monthly basis was retained and is fulfilled. Interestingly, the close temporal proximity of measurements from different spacecrafts suggest inter-calibration methods can be developed.

The mission lifetime requirement is driven by the need to cover at least one annual cycle. Therefore, a minimum mission lifetime of at least two years is required. As a secondary requirement, the mission lifetime would benefit from extension to 4 years in order to sample the El Nino Southern Oscillation and the quasi-biennial oscillation.

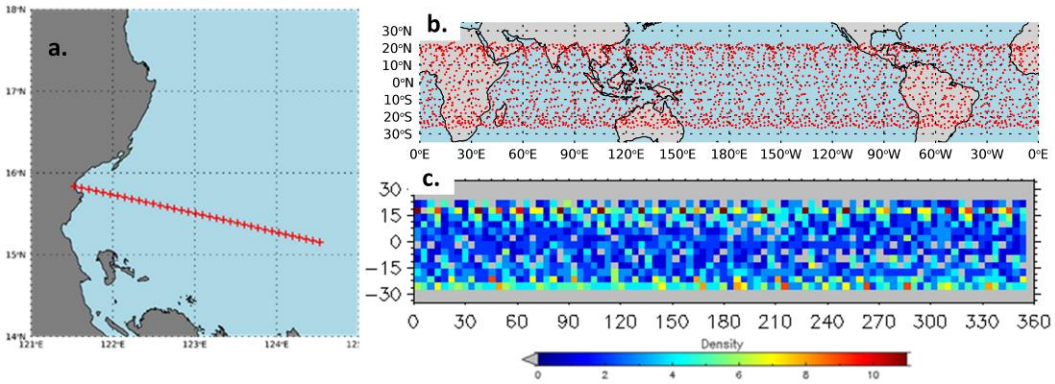

Figure 2. a) Illustration of the geographical spread of tangent height measurement during a single occultation event for a single spacecraft. Tangent height from 0 to 100 km are represented; b) Monthly coverage map of the constellation considering only the 30 km tangent height measurement; c) corresponding monthly coverage density map using the 4°x4° latitude longitude grid requirements. All these calculations were done for a nominal orbit of 520 km altitude and 28° inclination.

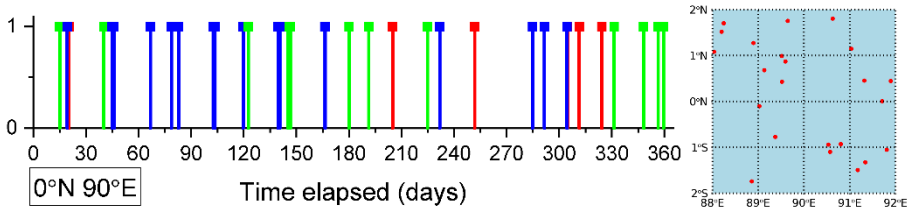

Figure 3. Analogous to a revisit time considering a 4°x4° cell and recording the measurement occurrences over a one month period. The stick colours refers to the three different satellites of the constellation. On the right hand side is shown the geographical position of the 30 km tangent point measured within the cell.

4. INSTRUMENT PAYLOAD

4.1 High resolution InfraRed Occultation Spectrometer (HIROS)

HIROS is an ultra-high spectral resolution laser heterodyne spectro-radiometer (LHR) inherited from laboratory and ground based instruments used for solar occultation atmospheric sounding. It's development for space mission started with the MISO mission[55].

The combined science and programmatic requirements call for innovative technologies allowing significant miniaturization whilst maintaining a high level of performance. The HIROS is based on quantum cascade laser local oscillator and optical photomixing using high speed photodiodes[56, 57]. The spectrometer relies on heterodyne (or coherent) detection, similar in its principles to coherent radio-receivers, but transposed in the optical domain. The measurement principle consists of measuring the amount of spectral power down-converted from the optical domain to radio-frequencies, in the vicinity of the local oscillator frequency and within a fixed filter bandwidth. By tuning the local oscillator continuously, the optical spectrum is resolved within the tuning range of the laser with noise ideally limited to the photon shot noise. This approach uniquely allows to obtain ultra-high spectral resolution in miniaturized packages, using hybrid optical integration technique based on hollow waveguides[58, 59]. Figure 4 shows a 3D model of the HIROS optical payload and its control electronics, and Table 1 provide some key generic specifications of the instrument.

The spectrometric technique brings two drawbacks that can be well mitigated: 1) the spectral coverage is defined by the tuning range of the local oscillator laser and therefore limited to few cm^{-1} windows when QCL are used. This is mitigated by targeting a few specific molecules within narrow spectral windows, selected from the sounding requirements and determined using observing system simulation for optimization of information content[55, 60]. 2) In its most compact form, spectral multiplexing is not viable. Therefore, spectral channels are acquired sequentially through a

frequency sweep of the local oscillator laser. This simple and cost effective sequential mode of operation nevertheless provides suitable SNR in LSO observing mode given the high brightness of the background source.

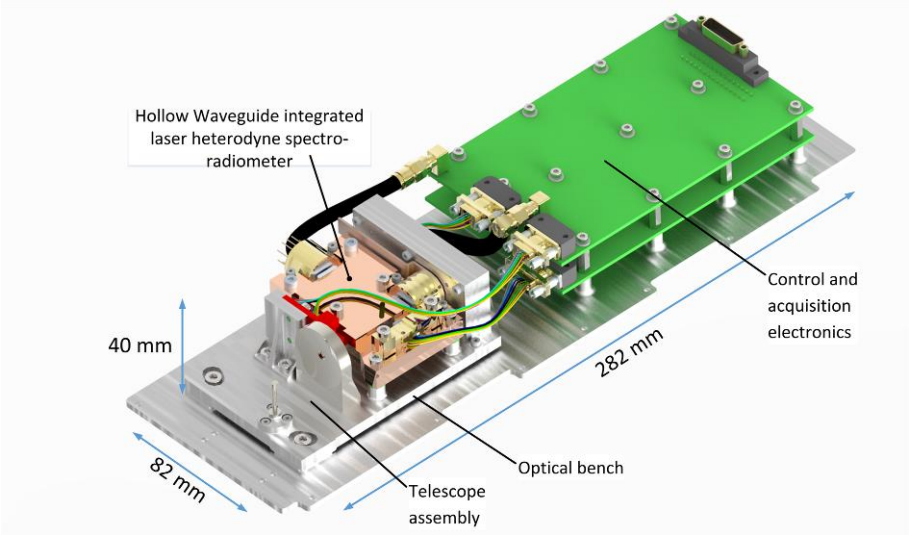

Figure 4. 3D CAD of the HIROS instrument. The front-end optics is a 1 inch diameter telescope coupling he incoming light into the integrated block containing the hollow waveguide integrated laser heterodyne spectro-radiometer. High speed photodiode electronics is at the back. The system is mounted on a breadboard that can be coaligned with other instruments' FoV part of the payload.

Each CubeMAP spacecraft will host three HIROS instruments. Identical except for the central wavelength of their local oscillators. Through atmospheric retrieval simulations, following a methodology already reported[61, 60, 55], three spectral windows were optimally selected:

- 1135.2 – 1134.2 cm-1 for O3, N2O, H2O, and CH3D

- 1239.2 - 1240.2 cm-1 for 13CH4, CH4, N218O, 15NNO, N2O, H2O, HDO and 18COC

- 1252.0 - 1253.0 cm-1 for 15NNO, N2O, CH4, 13CH4, HDO, 18COC

Table 1. Top level specifications of the HIROS instrument.

Parameter	Value	Comment
Volume Mass Power	1 dm3 1.3 kg 4Wh per orbit	The volume envelope is given in Figure 4. Mass includes margins. Power consumption peaks during eclipse only (~few minutes / orbit).
Spectral resolution	0.02–0.002 cm^{-1}	Enable line shapes resolution and improved spectral selectivity. Determined by RF filters switchable in orbit if multiple resolution is required.
SNR@8.5µm	>200	Key parameter in determining the sounding precision. Strongly dependent on integration time and resolution.
FOV	<0.5 mrad @ 25 mm dia.	Limited to a single spatial mode, therefore inherently small even with small optics. Dependent on mirror diameter.
Wavelength	8-12 µm	Central wavelength of laser can be tailored within this range. Once tailored, typically ~1 cm^{-1} narrow window are used.

4.2 Hyperspectral Solar Disc Imager (HSDI)

The HSDI fulfils two requirements. Primarily, a solar disk imager is required in order to ensure the required pointing knowledge of the spacecraft and reconstruct the sounding geometry: this is the prime function of the HSDI. As a secondary requirements, since the imager is required, by using a hyperspectral imager, additional science data useful to fulfil the science objectives can be obtained: aerosol extinction measurements, and oxygen A band measurements to derive pressure or air mass. Turning the solar disk imager into the HSDI cost-effectively adds a hyperspectral radiometer operating in the VIS/NIR to the instrument payload.

To fulfil the miniaturization and cost-effectiveness requirements enabling the constellation, a Multi Spectral Filter Array (MSFA) in place of a standard CMOS imager is used. CubeMAP uses a standard MSFA from IMEC based on CMOSIS CMV2000, made of 16 spectral channels with bandpass $\Delta\lambda$ of ~16 nm in the VIS/NIR. The filter responses are shown in Figure 5. A first performance analysis has been made based on the sensor specification, data from a laboratory ground-based demonstrator and retrieval simulations. The sensor will provide a noise equivalent transmission of 10^{-4} in each band. The bands are suitable for O2, H2O column retrieval, as well as aerosol extinction coefficients. Figure 5 shows the sensor spectral response together with a simulated 12 km tangent high atmospheric limb transmission. Unlike other aerosol remote sensing techniques such as lidars and limb scattering sensors, CubeMAP will measure the aerosol extinction directly and does not need any assumptions on the particle type and size distribution. This is therefore, the ultimate aerosol remote sensing solution for the UT/LS and the stratosphere.

The benefits of the approach retained for CubeMAP are twofold:

- The solar disc image can be analysed at full sensor pixel resolution (2048x1088) to deduce a highly accurate pointing knowledge to +/- 1 pixel resolution (5.5 micron in the sensor plane).
- 16 lower resolution images (512x272) can be extracted from the aliased mosaic image, and pixel averaging can be used to improve the SNR of the transmission measurement.

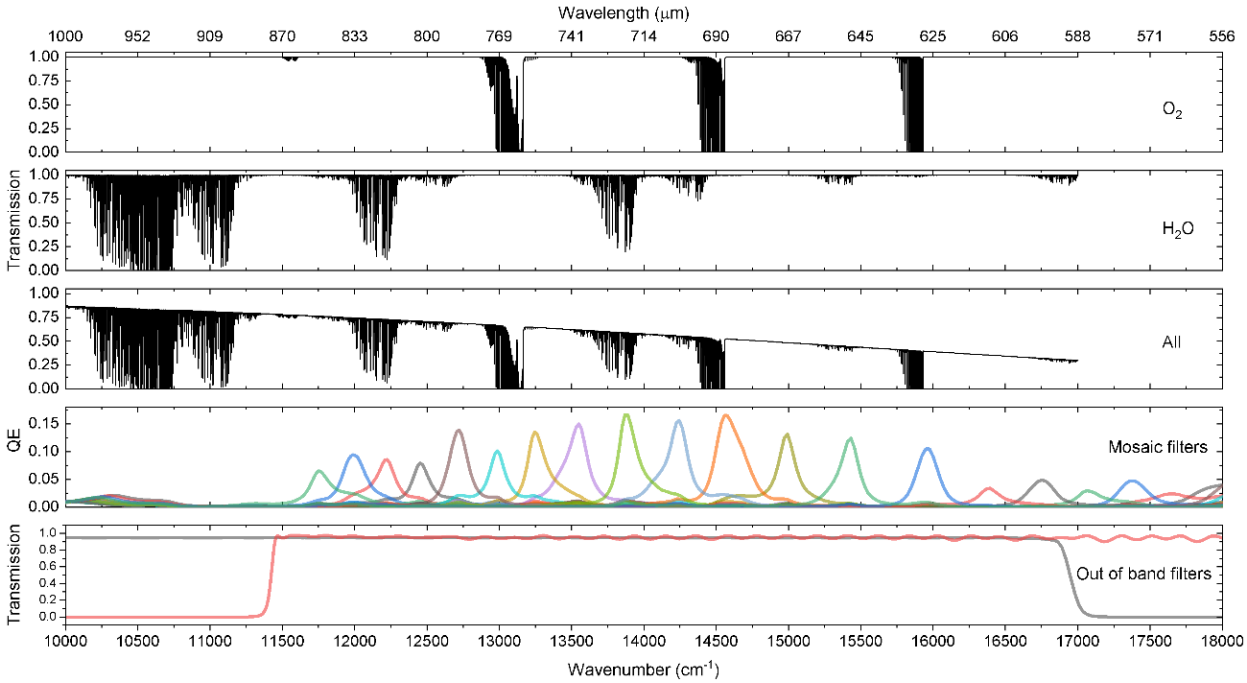

Figure 5. Illustration of the way the HSDI transmittance data are simulated. The atmospheric forward model produces the high resolution transmittance of the atmosphere given the viewing geometry (12 km tangent height in this example). Main absorbers in scope are water, oxygen and aerosols. The instrument is primarily characterized by the response of its 16 mosaic channels as well as the two out of band filters.

To image the sun onto the mosaic sensor, an achromatic doublet is used. The layout has been folded to ensure compactness and the correct position of the focal plane as shown in Figure 6. The folding is done in-plane, except for the last mirror that sent the beam to the sensor installed on the electronic board. The telescope is diffraction limited at all wavelengths. Due to the high f# (29) there is a correspondingly large depth of focus = ± 1 mm, which makes this design relatively insensitive to uniform thermal variations. The completed model of HSDI is shown in Figure 6. It fits in an envelope of 10x10x3.1 cm^3, weights 540 g (including margins) and consumes up 3.5 W in readout mode.

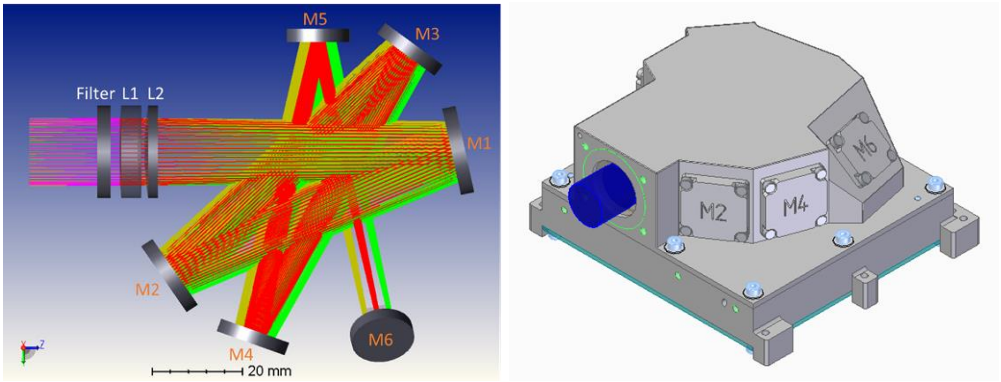

Figure 6. Left, schematic of the optical layout of the HSDI instrument. Right, CAD model of the completed, enclosed instrument.

5. THE CUBEMAP PLATFORM

The space segment of the CubeMAP mission is comprised of three identical spacecraft that interact with the Mission Operations Centre (MOC) through a commercial Ground Station Network (GSN). The satellites fly on the same orbit and they are equally spaced along it with a nominal difference in the mean anomaly of 120 deg. This provides a coverage and revisit time in accordance with the overall objectives of the mission.

Flight operation and control is handled by GomSpace Luxembourg operation centre using the Mega-Constellation Operations Platform (MCOP). Data processing is organised at the Centre for Environmental Data Analysis (CEDA) located on the Harwell Campus, Oxfordshire, UK. Long term data archival is anticipated to be at ESRIN (ESA's European Space Research Institute).

Each spacecraft is a 12U GomSpace CubeSat (2U x 2U x 3U) designed to accommodate the four different payloads (three HIROS instruments and one HSDI) and support their operations in order to achieve the mission objectives. Figure 7 depicts an artistic representation of the envisioned CubeMAP constellation.

Figure 7. CubeMAP constellation.

In order to achieve the mission objectives, a combination of GomSpace and third-party components are selected for the bus. The state of the art platform provides abundant payload volume, a precise Attitude and Orbit Control System (AOCS), a reliable power subsystem which can meet the required concept of operations, and a powerful communications subsystem with high data throughput.

As platform key characteristics, it is worth highlighting:

- Platform form factor: 12U (2U x 2U x 3U).
- Platform Flight Heritage: CubeMAP inherits and combines the experience of ESA's GOMX-3, GOMX-4, and GOMX-5 missions, as well as other commercial GomSpace projects.
- Mass: 17.87 kg, including component and system level margins according to ECSS policies.
- Power capabilities:
    - Orbit Average Power (OAP) ranging between 16.71 and 32.08 W, depending on the satellite attitude and the relative geometry between the orbit and the Sun.
    - Maximum Depth of Discharge (DoD) of the batteries of <20% at Beginning of Life (BOL), which ensures the platform reliability for the required lifetime.
    - Power budget compatible with the required concept of operations comprising two occultation experiments per orbit and four ground station passes per day.
- AOCS: GomSpace advanced AOCS components, including a star tracker (Hyperion ST200) for fine attitude determination and an electric propulsion system (Enpulsion IFM NanoThruster) for orbit control.
- Pointing accuracy: in Local Vertical Local Horizontal (LVLH) mode: < 0.1 degree @ 3σ in all three axes.
- Internal data storage capabilities:
    - On-board computer: 512 MB (considerably higher than the retrieved housekeeping data, flight plans and memory used by the applications).
    - Software Defined Radio (SDR): up to 32 GB.
- Communications subsystems:

    - Low rate TMTC subsystem comprising a GomSpace NanoCom AX2150 radio and a quasi-omnidirectional antenna. This system is to be used during the critical phases of the mission (LEOP and while the satellite is in safe mode) with data rate of 19.2 kbps (configurable) and uplink/downlink capabilities of 2.16 MB/day.
    - High Speed Link (HSL) subsystem which relies on the flight proven GomSpace NanoCom SR2000 and the NanoCom ANT2150 with data rate of 7 Mbps (configurable) and uplink/downlink capabilities of 788.12 MB/day.
- Delta-V capabilities: up to 213 m/s, depending on the operational point of the thruster.
- Qualification: All qualified components have undergone the GomSpace qualification program which complies with a broad range of launch vehicles (NASA GEVS is used as reference). On-going product developments are undergoing the same program.
- Deployer: The 12U platform is being designed to comply with the majority of commercial PODs available on the market.

5.1 CubeMAP Spacecraft Subsystems

This section provides a high-level description of the platform bus subsystems.

5.1.1 Mechanical and utilities

The mechanical subsystem comprises a 12U (2Ux2Ux3U) structure, external cover plates and a Flight Preparation Panel (FPP), used for on-ground battery charging and data interface. The 12U structure is an on-going development by GomSpace which will also be used for ESA's GOMX-5 mission. The structure relies on the heritage of the GomSpace 6U platform and aims to optimise the subsystems integration and the volume utilisation whilst ensuring the satellite integrity.

5.1.2 Attitude and Orbit Control system / Guidance Navigation and control

The advanced AOCS of the CubeMAP satellite is responsible for spacecraft pointing and stability. The ADCS computer, known as the NanoDock ADCS-6, is designed with two daughterboards: the ADCS computer (based on the NanoMind A3200) and the NovAtel OEM719 GNSS receiver. The computer is equipped with GomSpace ADCS software package which has extensive flight heritage and only requires to be tailored to the specific configuration of the CubeMAP mission.

The system uses six NanoSense Fine Sun Sensors (one on each face), the NanoSense M315 3-axis magnetometer, Sensonor STIM210 gyroscope and Hyperion ST200 star tracker for primary Attitude Determination. The internal magnetometer on the ADCS computer works as backup to the NanoSense M315 and the internal gyro on the ADCS computer works as backup for the STIM210, providing redundancy.

For Attitude Control, four GSW-600 wheels in a pyramid configuration are used, with a single wheel redundancy. The proposed system has an accuracy of less than 0.1 degree @ 3σ pointing error in all three axes.

For Orbit Determination, the spacecraft can use two different inputs:

- The Novatel OEM719 GNSS receiver is used together with the Tallysman TW1322 antenna covering both Global Positioning System (GPS) L1 and Glonass.
- Two-Line Elements (TLEs) are provided from the ground station on a periodic basis and propagated on-board using a SGP4 model.

Active Orbit Control is achieved using the Enpulsion IFM NanoThruster, an electric-propulsion system designed for CubeSats with flight heritage and the capacity of meeting the mission requirements.

5.1.3 Electronic Power Systems

The power subsystem provides the power generation, power distribution and energy storage functions to the spacecraft. The system is designed to:

- Collect energy from the solar panels and convert it to system voltage.
- Charge the batteries and maintain batteries in healthy conditions.
- Convert system voltage to lower voltage fitted payloads.
- Protect and provide power distribution for payloads.
- System monitoring and power management.

The system is comprised of one NanoPower BPX battery pack for energy storage; one NanoPower P60 for energy conditioning and distribution with one NanoPower Array Conditioning Units (ACUs) and three NanoPower Power Distribution Units (PDUs); and a combination of body-mounted and deployable solar panels to generate power.

5.1.4 Command & Data-handling Systems

The C&DH system makes use of the NanoMind A3200 as On-Board Computer (OBC) and GomSpace mission software. Apart from collecting housekeeping data and tasking other subsystems, the C&DH has a health monitoring application to act as Failure Detection Isolation and Recovery (FDIR) subsystem. The NanoMind A3200 has extensive flight heritage and is thus a space proven system. The A3200 daughterboard is accommodated on the NanoDock DMC-3 motherboard together with the NanoCom AX2150 S-Band Radio.

5.1.5 Communications

The CubeMAP spacecraft has two communications subsystems: one for near-omnidirectional S-Band links used during LEOP and as back-up, and one for S-Band HSL used during nominal operations.

- LEOP/Back-up subsystem:
    - This subsystem comprises the NanoCom AX2150 S-Band radio and a S-Band quasi omni-directional antenna providing a close-to-spherical radiation pattern. The AX2150 daughterboard is accommodated on the DMC-3 motherboard together with the A3200 onboard computer (OBC). The TMTC specific S-Band up and downlink are planned to be used for telemetry and commands only during LEOP and for backup purposes (afterwards TMTC data will be sent over the standard HSL).
- HSL subsystem:
    - The HSL communications subsystem is comprised of a S-Band Antenna for HSL named NanoCom ANT2150 and a Software Defined Radio (SDR) called NanoCom SR2000. The GomSpace NanoCom ANT2150 is an active antenna specifically designed for interfacing with GomSpace SDR transceivers. The NanoCom ANT-2150-DUP is a full duplex antenna with RX in 2025-2110 MHz and TX in 2200-2290 MHz. The SR2000 system is based on the flight proven NanoCom SDR platform which comprises one motherboard called NanoDock SDR and two daughterboards: a NanoMind Z7000 computer and a NanoCom TR600 radio.

5.2 CubeMAP spacecraft configuration

As shown in Figure 8, the external faces of the spacecraft are covered by deployable (NanoPower DSP) and body-mounted (NanoPower MSP) solar panels and cover plates. Both low-rate TMTC (S-Band omni antenna) and HSL (NanoCom ANT2150) antennas are placed on one of the 4U sides of the spacecraft (+Z) together with the openings for the payloads' fields of view. The Flight Preparation Panel is accommodated on the opposite 4U face (-Z) with the star tracker (Hyperion ST200) field of view and the electric propulsion thruster (Enpulsion IFM NanoThruster). The two deployable solar panels are stowed on the ±X faces and deployed after launch, pointing towards +Y. The +Y side is used to accommodate a 16-cell body mounted solar panel (NanoPower MSP), whilst the remaining faces are used as radiators to ensure that the payloads remain within their required temperature range.

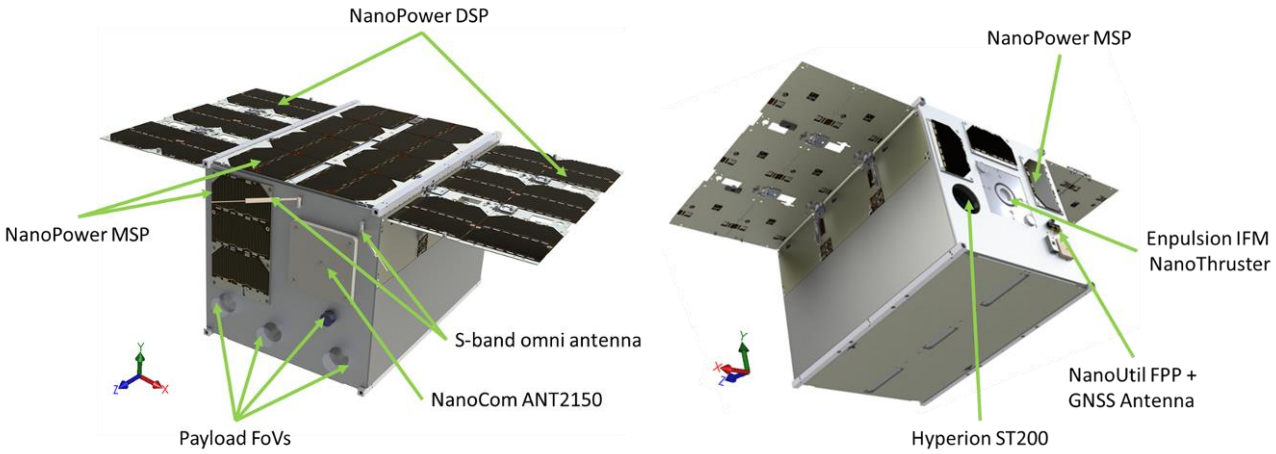

Figure 8. Left, CubeMAP spacecraft external view, +Z face. Right, CubeMAP spacecraft external view, -Z face.

Figure 9 shows the internal layout of the platform bus components (the top wall has been removed in order to have a better view of the distribution of the different parts). All the avionics components (except for the propulsion system and the star tracker) are located on the top 6U volume (i.e. facing the +Y side of the satellite). The bottom 6U are allocated for the payload. This configuration guarantees that the payload is in contact with the cold face of the spacecraft with a more stable thermal behaviour.

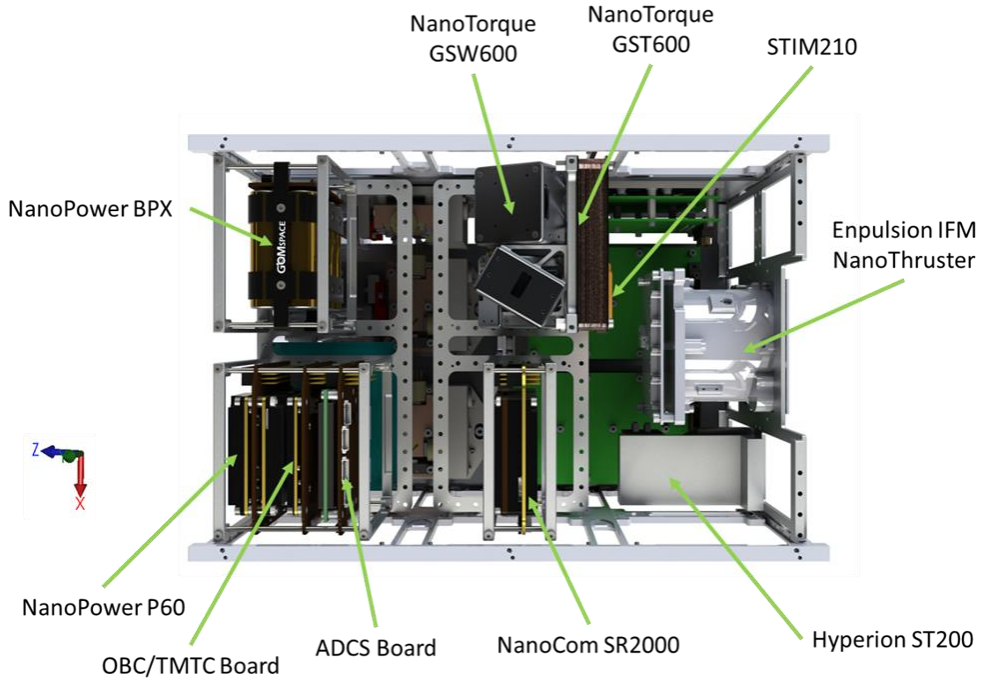

Figure 9. CubeMAP spacecraft internal view.

5.3 CubeMAP spacecraft summary

The GomSpace 12U spacecraft proposed for the CubeMAP mission provides all the resources required to meet the mission objectives and requirements. The platform ensures the integrity of the payload and the bus components, provides

a good thermal interface so that all subsystems are within their acceptable range, and it provides all electrical, software and mechanical interfaces. It is a mature spacecraft given that the avionics rely on flight proven components and the on-going product developments inherit the experience from existing systems and will reach TRL 9 before the launch date expected for CubeMAP.

6. CONCLUSION

The science case and some of space segment elements of the CubeMAP mission currently being consolidated in the context of the ESA SCOUT programme have been briefly presented. CubeMAP focuses on the monitoring of middle atmospheric processes in the tropics, though high-resolution thermal infrared spectroscopy in the limb, using the sun as a background. High spectral resolution infrared spectroscopy of atmospheric constituents of the middle atmosphere, resolving Doppler limited lines, is usually achievable by very large instrument payload incompatible with nanosatellite platforms. CubeMAP obviates these limitations for the first time. As a result, the traditional lack of spatial coverage inherent to limb solar occultation can be mitigated through constellation flying, hence offering an excellent trade-off in terms of coverage, sounding accuracy, and cost.

In addition to its immediate scientific objectives, CubeMAP contributes to developing a novel resilient approach to atmospheric observation: it offers a high level of deployment flexibility and system modularity, as well as economy of scale, through the use of identical payloads and platforms but targeted towards specific Earth observation goals. CubeMAP is highly complementary to the existing nadir sounding infrastructure and will add value by enhancing its outputs and exploitation. It also addresses the forthcoming critical gap in solar occultation sounding capabilities that is inevitable if this mission is not flown.

REFERENCES

[1] Fueglistaler, S., Dessler, A. E., Dunkerton, T. J., Folkins, I., Fu, Q. and Mote, P. W., "Tropical tropopause layer," Rev. Geophys. **47**(1), RG1004 (2009).

[2] Boucher, O., Randall, D., Artaxo, P., Bretherton, C., Feingold, G., Forster, P., Kerminen, V.-M., Kondo, Y., Liao, H., Lohmann, U., Rasch, P., Satheesh, S. K., Sherwood, S., Stevens, B. and Zhang, X. Y., "Clouds and Aerosols," [Climate Change 2013 - The Physical Science Basis], Intergovernmental Panel on Climate Change, Ed., Cambridge University Press, Cambridge, 571–658 (2013).

[3] Riese, M., Ploeger, F., Rap, A., Vogel, B., Konopka, P., Dameris, M. and Forster, P., "Impact of uncertainties in atmospheric mixing on simulated UTLS composition and related radiative effects," J. Geophys. Res. Atmos. **117**(D16), n/a-n/a (2012).

[4] Gettelman, a., Hoor, P., Pan, L. L., Randel, W. J., Hegglin, M. I. and Birner, T., "THE EXTRATROPICAL UPPER TROPOSPHERE AND LOWER STRATOSPHERE," Rev. Geophys. **49**(3), RG3003 (2011).

[5] Karpechko, A. Y., Hitchcock, P., Peters, D. H. W. and Schneidereit, A., "Predictability of downward propagation of major sudden stratospheric warmings," Q. J. R. Meteorol. Soc. **143**(704), 1459–1470 (2017).

[6] Domeisen, D. I. V., Butler, A. H., Charlton-Perez, A. J., Ayarzagüena, B., Baldwin, M. P., Dunn-Sigouin, E., Furtado, J. C., Garfinkel, C. I., Hitchcock, P., Karpechko, A. Y., Kim, H., Knight, J., Lang, A. L., Lim, E., Marshall, A., Roff, G., Schwartz, C., Simpson, I. R., Son, S., et al., "The Role of the Stratosphere in Subseasonal to Seasonal Prediction: 1. Predictability of the Stratosphere," J. Geophys. Res. Atmos. **125**(2), 1–17 (2020).

[7] Kidston, J., Scaife, A. A., Hardiman, S. C., Mitchell, D. M., Butchart, N., Baldwin, M. P. and Gray, L. J., "Stratospheric influence on tropospheric jet streams, storm tracks and surface weather," Nat. Geosci. **8**(6), 433–440 (2015).

[8] Hossaini, R., Chipperfield, M. P., Montzka, S. A., Rap, A., Dhomse, S. and Feng, W., "Efficiency of short-lived halogens at influencing climate through depletion of stratospheric ozone," Nat. Geosci. **8**(3), 186–190 (2015).

[9] Randel, W. J., Park, M., Emmons, L., Kinnison, D., Bernath, P., Walker, K. A., Boone, C. and Pumphrey, H., "Asian Monsoon Transport of Pollution to the Stratosphere," Science (80-.). **328**(5978), 611–613 (2010).

[10] Son, S.-W., Han, B.-R., Garfinkel, C. I., Kim, S.-Y., Park, R., Abraham, N. L., Akiyoshi, H., Archibald, A. T., Butchart, N., Chipperfield, M. P., Dameris, M., Deushi, M., Dhomse, S. S., Hardiman, S. C., Jöckel, P., Kinnison, D., Michou, M., Morgenstern, O., O'Connor, F. M., et al., "Tropospheric jet response to Antarctic ozone depletion: An update with Chemistry-Climate Model Initiative (CCMI) models," Environ. Res. Lett. **13**(5), 054024 (2018).

[11] Bandoro, J., Solomon, S., Donohoe, A., Thompson, D. W. J. and Santer, B. D., "Influences of the Antarctic Ozone Hole on Southern Hemispheric Summer Climate Change," J. Clim. **27**(16), 6245–6264 (2014).

[12] Solomon, S., Rosenlof, K. H., Portmann, R. W., Daniel, J. S., Davis, S. M., Sanford, T. J. and Plattner, G.-K., "Contributions of Stratospheric Water Vapor to Decadal Changes in the Rate of Global Warming," Science (80-.). **327**(5970), 1219–1223 (2010).

[13] Seidel, D. J., Gillett, N. P., Lanzante, J. R., Shine, K. P. and Thorne, P. W., "Stratospheric temperature trends: our evolving understanding," Wiley Interdiscip. Rev. Clim. Chang. **2**(4), 592–616 (2011).

[14] Maycock, A. C., Joshi, M. M., Shine, K. P., Davis, S. M. and Rosenlof, K. H., "The potential impact of changes in lower stratospheric water vapour on stratospheric temperatures over the past 30 years," Q. J. R. Meteorol. Soc. **140**(684), 2176–2185 (2014).

[15] Hegglin, M. I., Plummer, D. A., Shepherd, T. G., Scinocca, J. F., Anderson, J., Froidevaux, L., Funke, B., Hurst, D., Rozanov, A., Urban, J., von Clarmann, T., Walker, K. A., Wang, H. J., Tegtmeier, S. and Weigel, K., "Vertical structure of stratospheric water vapour trends derived from merged satellite data," Nat. Geosci. **7**(10), 768–776 (2014).

[16] Randel, W. J., Wu, F., Vömel, H., Nedoluha, G. E. and Forster, P., "Decreases in stratospheric water vapor after 2001: Links to changes in the tropical tropopause and the Brewer-Dobson circulation," J. Geophys. Res. **111**(D12), D12312 (2006).

[17] Revell, L. E., Stenke, A., Rozanov, E., Ball, W., Lossow, S. and Peter, T., "The role of methane in projections of 21st century stratospheric water vapour," Atmos. Chem. Phys. **16**(20), 13067–13080 (2016).

[18] Randel, W. J. and Jensen, E. J., "Physical processes in the tropical tropopause layer and their roles in a changing climate," Nat. Geosci. **6**(3), 169–176 (2013).

[19] Hegglin, M. I. and Shepherd, T. G., "Large climate-induced changes in ultraviolet index and stratosphere-to-troposphere ozone flux," Nat. Geosci. **2**(10), 687–691 (2009).

[20] Randel, W. J., Wu, F. and Forster, P., "The Extratropical Tropopause Inversion Layer: Global Observations with GPS Data, and a Radiative Forcing Mechanism," J. Atmos. Sci. **64**(12), 4489–4496 (2007).

[21] Kunkel, D., Hoor, P. and Wirth, V., "The tropopause inversion layer in baroclinic life-cycle experiments: the role of diabatic processes," Atmos. Chem. Phys. **16**(2), 541–560 (2016).

[22] Gettelman, A., Hegglin, M. I., Son, S.-W., Kim, J., Fujiwara, M., Birner, T., Kremser, S., Rex, M., Añel, J. A., Akiyoshi, H., Austin, J., Bekki, S., Braesike, P., Brühl, C., Butchart, N., Chipperfield, M., Dameris, M., Dhomse, S., Garny, H., et al., "Multimodel assessment of the upper troposphere and lower stratosphere: Tropics and global trends," J. Geophys. Res. **115**(20), D00M08 (2010).

[23] Wang, T., Zhang, Q., Lossow, S., Chafik, L., Risi, C., Murtagh, D. and Hannachi, A., "Stable Water Isotopologues in the Stratosphere Retrieved from Odin/SMR Measurements," Remote Sens. **10**(2), 166 (2018).

[24] Hersbach, H., Bell, B., Berrisford, P., Hirahara, S., Horányi, A., Muñoz-Sabater, J., Nicolas, J., Peubey, C., Radu, R., Schepers, D., Simmons, A., Soci, C., Abdalla, S., Abellan, X., Balsamo, G., Bechtold, P., Biavati, G., Bidlot, J., Bonavita, M., et al., "The ERA5 global reanalysis," Q. J. R. Meteorol. Soc.(September 2019), qj.3803 (2020).

[25] Simmons, A., Soci, C., Nicolas, J., Bell, B., Berrisford, P., Dragani, R., Flemming, J., Haimberger, L., Healy, S., Hersbach, H., Horányi, A., Inness, A., Munoz-Sabater, J., Radu, R. and Schepers, D., "Global stratospheric temperature bias and other stratospheric aspects of ERA5 and ERA5.1" (2020).

[26] Shepherd, T. G., Polichtchouk, I., Hogan, R. and Simmons, A. J., "Report on Stratosphere Task Force" (2018).

[27] Steinbrecht, W., Froidevaux, L., Fuller, R., Wang, R., Anderson, J., Roth, C., Bourassa, A., Degenstein, D., Damadeo, R., Zawodny, J., Frith, S., McPeters, R., Bhartia, P., Wild, J., Long, C., Davis, S., Rosenlof, K., Sofieva, V., Walker, K., et al., "An update on ozone profile trends for the period 2000 to 2016," Atmos. Chem. Phys. **17**(17), 10675–10690 (2017).

[28] Solomon, S., Ivy, D. J., Kinnison, D., Mills, M. J., Neely, R. R. and Schmidt, A., "Emergence of healing in the Antarctic ozone layer," Science (80-.). **353**(6296), 269–274 (2016).

[29] Ball, W. T., Alsing, J., Mortlock, D. J., Staehelin, J., Haigh, J. D., Peter, T., Tummon, F., Stübi, R., Stenke, A., Anderson, J., Bourassa, A., Davis, S. M., Degenstein, D., Frith, S., Froidevaux, L., Roth, C., Sofieva, V., Wang, R., Wild, J., et al., "Evidence for a continuous decline in lower stratospheric ozone offsetting ozone layer recovery," Atmos. Chem. Phys. **18**(2), 1379–1394 (2018).

[30] Ball, W. T., Alsing, J., Staehelin, J., Davis, S. M., Froidevaux, L. and Peter, T., "Stratospheric ozone trends for 1985–2018: sensitivity to recent large variability," Atmos. Chem. Phys. **19**(19), 12731–12748 (2019).

[31] Chipperfield, M. P., Dhomse, S., Hossaini, R., Feng, W., Santee, M. L., Weber, M., Burrows, J. P., Wild, J. D., Loyola, D. and Coldewey-Egbers, M., "On the Cause of Recent Variations in Lower Stratospheric Ozone," Geophys. Res. Lett. **45**(11), 5718–5726 (2018).

[32] Wargan, K., Orbe, C., Pawson, S., Ziemke, J. R., Oman, L. D., Olsen, M. A., Coy, L. and Emma Knowland, K., "Recent Decline in Extratropical Lower Stratospheric Ozone Attributed to Circulation Changes," Geophys. Res. Lett. **45**(10), 5166–5176 (2018).

[33] Butchart, N., Austin, J., Knight, J. R., Scaife, A. A. and Gallani, M. L., "The Response of the Stratospheric Climate to Projected Changes in the Concentrations of Well-Mixed Greenhouse Gases from 1992 to 2051," J. Clim. **13**(13), 2142–2159 (2000).

[34] McLandress, C. and Shepherd, T. G., "Simulated Anthropogenic Changes in the Brewer–Dobson Circulation, Including Its Extension to High Latitudes," J. Clim. **22**(6), 1516–1540 (2009).

[35] Corrêa, M. D. P., Godin-Beekmann, S., Haeffelin, M., Bekki, S., Saiag, P., Badosa, J., Jégou, F., Pazmiño, A. and Mahé, E., "Projected changes in clear-sky erythemal and vitamin D effective UV doses for Europe over the period 2006 to 2100," Photochem. Photobiol. Sci. **12**(6), 1053 (2013).

[36] Lamy, K., Portafaix, T., Josse, B., Brogniez, C., Godin-Beekmann, S., Bencherif, H., Revell, L., Akiyoshi, H., Bekki, S., Hegglin, M. I., Jöckel, P., Kirner, O., Liley, B., Marecal, V., Morgenstern, O., Stenke, A., Zeng, G., Abraham, N. L., Archibald, A. T., et al., "Clear-sky ultraviolet radiation modelling using output from the Chemistry Climate Model Initiative," Atmos. Chem. Phys. **19**(15), 10087–10110 (2019).

[37] Intergovernmental Panel on Climate Change, ed., "Anthropogenic and Natural Radiative Forcing," [Climate Change 2013 - The Physical Science Basis], Cambridge University Press, Cambridge, 659–740 (2014).

[38] Cionni, I., Eyring, V., Lamarque, J. F., Randel, W. J., Stevenson, D. S., Wu, F., Bodeker, G. E., Shepherd, T. G., Shindell, D. T. and Waugh, D. W., "Ozone database in support of CMIP5 simulations: results and corresponding radiative forcing," Atmos. Chem. Phys. **11**(21), 11267–11292 (2011).

[39] Checa-Garcia, R., Hegglin, M. I., Kinnison, D., Plummer, D. A. and Shine, K. P., "Historical Tropospheric and Stratospheric Ozone Radiative Forcing Using the CMIP6 Database," Geophys. Res. Lett. **45**(7), 3264–3273 (2018).

[40] Saad, K. M., Wunch, D., Deutscher, N. M., Griffith, D. W. T., Hase, F., De Mazière, M., Notholt, J., Pollard, D. F., Roehl, C. M., Schneider, M., Sussmann, R., Warneke, T. and Wennberg, P. O., "Seasonal variability of stratospheric methane: implications for constraining tropospheric methane budgets using total column observations," Atmos. Chem. Phys. **16**(21), 14003–14024 (2016).

[41] Streets, D. G., Canty, T., Carmichael, G. R., de Foy, B., Dickerson, R. R., Duncan, B. N., Edwards, D. P., Haynes, J. A., Henze, D. K., Houyoux, M. R., Jacob, D. J., Krotkov, N. A., Lamsal, L. N., Liu, Y., Lu, Z., Martin, R. V, Pfister, G. G., Pinder, R. W., Salawitch, R. J., et al., "Emissions estimation from satellite retrievals: A review of current capability," Atmos. Environ. **77**, 1011–1042 (2013).

[42] Houweling, S., Bergamaschi, P., Chevallier, F., Heimann, M., Kaminski, T., Krol, M., Michalak, A. M. and Patra, P., "Global inverse modeling of CH4 sources and sinks: An overview of methods," Atmos. Chem. Phys. **17**(1), 235–256 (2017).

[43] Gaudel, A., Cooper, O. R., Ancellet, G., Barret, B., Boynard, A., Burrows, J. P., Clerbaux, C., Coheur, P. F., Cuesta, J., Cuevas, E., Doniki, S., Dufour, G., Ebojie, F., Foret, G., Garcia, O., Granados Muños, M. J., Hannigan, J. W., Hase, F., Huang, G., et al., "Tropospheric Ozone Assessment Report: Present-day distribution and trends of tropospheric ozone relevant to climate and global atmospheric chemistry model evaluation," Elem Sci Anth **6**(1), 39 (2018).

[44] Shepherd, T. G., Plummer, D. A., Scinocca, J. F., Hegglin, M. I., Fioletov, V. E., Reader, M. C., Remsberg, E., von Clarmann, T. and Wang, H. J., "Reconciliation of halogen-induced ozone loss with the total-column ozone record," Nat. Geosci. **7**, 443 (2014).

[45] Hegglin, M. I., Brunner, D., Peter, T., Hoor, P., Fischer, H., Staehelin, J., Krebsbach, M., Schiller, C., Parchatka, U. and Weers, U., "Measurements of NO, NO_y, N_2O, and O_3 during SPURT: implications for transport and chemistry in the lowermost stratosphere," Atmos. Chem. Phys. **6**(5), 1331–1350 (2006).

[46] Schoeberl, M. R., Duncan, B. N., Douglass, A. R., Waters, J., Livesey, N., Read, W. and Filipiak, M., "The carbon monoxide tape recorder," Geophys. Res. Lett. **33**(12), L12811 (2006).

[47] Folkins, I., Bernath, P., Boone, C., Lesins, G., Livesey, N., Thompson, A. M., Walker, K. and Witte, J. C., "Seasonal cycles of O 3 , CO, and convective outflow at the tropical tropopause," Geophys. Res. Lett. **33**(16), L16802 (2006).

[48] Khaykin, S. M., Godin-Beekmann, S., Hauchecorne, A., Pelon, J., Ravetta, F. and Keckhut, P., "Stratospheric Smoke With Unprecedentedly High Backscatter Observed by Lidars Above Southern France," Geophys. Res. Lett. **45**(3), 1639–1646 (2018).

[49] Vernier, J.-P., Fairlie, T. D., Natarajan, M., Wienhold, F. G., Bian, J., Martinsson, B. G., Crumeyrolle, S., Thomason, L. W. and Bedka, K. M., "Increase in upper tropospheric and lower stratospheric aerosol levels and its potential connection with Asian pollution," J. Geophys. Res. Atmos. **120**(4), 1608–1619 (2015).

[50] Müller, S., Hoor, P., Bozem, H., Gute, E., Vogel, B., Zahn, A., Bönisch, H., Keber, T., Krämer, M., Rolf, C., Riese, M., Schlager, H. and Engel, A., "Impact of the Asian monsoon on the extratropical lower stratosphere: trace gas observations during TACTS over Europe 2012," Atmos. Chem. Phys. **16**(16), 10573–10589 (2016).

[51] Vogel, B., Günther, G., Müller, R., Grooß, J.-U., Afchine, A., Bozem, H., Hoor, P., Krämer, M., Müller, S., Riese, M., Rolf, C., Spelten, N., Stiller, G. P., Ungermann, J. and Zahn, A., "Long-range transport pathways of tropospheric source gases originating in Asia into the northern lower stratosphere during the Asian monsoon season 2012," Atmos. Chem. Phys. **16**(23), 15301–15325 (2016).

[52] Russell, J. M., "Satellite solar occultation sounding of the middle atmosphere," Pure Appl. Geophys. PAGEOPH **118**(1), 616–635 (1980).

[53] Mero, B., Quillien, K. A., Mcrobb, M., Chesi, S., Marshall, R., Gow, A. and Clark, C., "PICASSO: A State of the Art CubeSat," 29th Annu. AIAA/USU Conf. Small Satell., 1–8 (2015).

[54] Bevilacqua, R. M., Fromm, M. D., Bailey, S. M., Fish, C. S. and Gordley, L. L., "SSC15-XII-3 Solar Occultation Constellation for Retrieving Aerosols and Trace Element Species (SOCRATES) Mission Concept," 29th Annu. AIAA/USU Conf. small Satell. (2015).

[55] Weidmann, D., Hoffmann, A., Macleod, N., Middleton, K., Kurtz, J., Barraclough, S. and Griffin, D., "The Methane Isotopologues by Solar Occultation (MISO) Nanosatellite Mission: Spectral Channel Optimization and Early Performance Analysis," Remote Sens. **9**(10), 1073 (2017).

[56] Weidmann, D., Reburn, W. J. and Smith, K. M., "Ground-based prototype quantum cascade laser heterodyne radiometer for atmospheric studies," Rev. Sci. Instrum. **78**(7), 073107 (2007).

[57] Weidmann, D., Tsai, T., Macleod, N. a and Wysocki, G., "Atmospheric observations of multiple molecular species using ultra-high-resolution external cavity quantum cascade laser heterodyne radiometry," Opt. Lett. **36**(11), 1951 (2011).

[58] Weidmann, D., Perrett, B. J., Macleod, N. a and Jenkins, R. M., “Hollow waveguide photomixing for quantum cascade laser heterodyne spectro-radiometry,” Opt. Express **19**(10), 9074 (2011).

[59] Robinson, I., Butcher, H. L., Macleod, N. A. and Weidmann, D., “Hollow waveguide integrated laser spectrometer for 13 CO 2 / 12 CO 2 analysis,” Opt. Express **27**(24), 35670 (2019).

[60] Smith, F., Havemann, S., Hoffmann, A., Bell, W., Weidmann, D. and Newman, S., “Evaluation of laser heterodyne radiometry for numerical weather prediction applications,” Q. J. R. Meteorol. Soc. **144**(715), 1831–1850 (2018).

[61] Hoffmann, A., Macleod, N. A., Huebner, M. and Weidmann, D., “Thermal infrared laser heterodyne spectroradiometry for solar occultation atmospheric CO2 measurements,” Atmos. Meas. Tech. **9**(12), 5975–5996 (2016).